Chemical tuning of a honeycomb magnet through a critical point

Austin M. Ferrenti [1,2,*] Maxime A. Siegler,[1] Shreenanda Ghosh,[2] Xin Zhang,[3] Nina Kintop,[4] Hector K. Vivanco,[1,2]
Chris Lygouras [2] Thomas Halloran [2,5] Sebastian Klemenz [4] Collin Broholm,[2,5]
Natalia Drichko,[2] and Tyrel M. McQueen[1,2,6,†]

[1]*Department of Chemistry, The Johns Hopkins University, Baltimore, Maryland 21218, USA*

[2]*Institute for Quantum Matter, William H. Miller III Department of Physics and Astronomy,*
The Johns Hopkins University, Baltimore, Maryland 21218, USA

[3]*Department of Chemical and Biomolecular Engineering, The Johns Hopkins University, Baltimore, Maryland 21218, USA*

[4]*Fraunhofer Research Institution for Materials Recycling and Resource Strategies IWKS,*
Aschaffenburger Straße 121, 64357 Hanau, Germany

[5]*NIST Center for Neutron Research, Gaithersburg, Maryland 20899, USA*

[6]*Department of Materials Science and Engineering, The Johns Hopkins University, Baltimore, Maryland 21218, USA*

$BaCo_2(AsO_4)_2$ (BCAO) has seen extensive study since its initial identification as a proximate Kitaev quantum spin liquid candidate. Thought to be described by the highly anisotropic XXZ-J_1-J_3 model, the ease with which magnetic order is suppressed in the system indicates proximity to a spin liquid phase. Upon chemical tuning via partial arsenic substitution with vanadium, we show an initial suppression of long-range incommensurate order in the BCAO system to $T \approx 3.0$ K, followed by increased spin freezing at higher substitution levels. Between these two regions, at around 10% substitution, the system is shown to pass through a critical point where the competing J_1/J_3 exchange interactions become more balanced, producing a more complex magnetic ground state, likely stabilized by quantum fluctuations. This state shows how slight compositional change in magnetically frustrated systems may be leveraged to tune ground state degeneracies and potentially realize a quantum spin liquid state.

DOI: 10.1103/PhysRevB.108.064433

I. INTRODUCTION

In the development of materials possessing improved mechanical, optoelectronic, and magnetic properties, small compositional changes can radically change the behaviors exhibited. To address long-standing scientific challenges—such as the stabilization of typically fragile, long-range spin entanglement in a real quantum spin liquid (QSL)—subtle modifications to promising, yet ultimately flawed candidates may be necessary [1,2]. The chemical tuning of a magnetic system, particularly where there exists a high degree of spin frustration, can provide a broader understanding of the competing exchange interactions which determine the degeneracy of the magnetic ground state and often results in the discovery of exotic quantum phenomena [3]. While direct substitution on the magnetic sublattice can yield important information about the type and magnitude of exchange occurring in a material, the realization of a stable spin liquid state in a magnetically frustrated system requires a more thorough understanding of other structural features that help mediate magnetic exchange. This is especially relevant for phases mimicking the prototypical Kitaev spin liquid (KQSL), where $S = 1/2$ moments on the vertices of a honeycomb lattice ex-perience only highly anisotropic, Ising-type interactions [4,5]. The bond-dependent nature of Kitaev exchange interactions makes such systems particularly sensitive to minor structural change.

One of the most intensely studied honeycomb spin liquid candidates, $BaCo_2(AsO_4)_2$, consists of d^7, octahedrally coordinated Co^{2+} ions, possessing a pseudospin-1/2 ground state doublet [6]. The honeycomb lattice in $BaCo_2(AsO_4)_2$, or BCAO, consists of edge-sharing, lightly distorted CoO_6 octahedra, which are believed to account for the high degree of planar anisotropy observed in its magnetic behavior at low temperatures [Figs. 1(a)–1(c)] [7]. BCAO orders antiferromagnetically at $T_N = 5.4$ K, with dominant in-plane ferromagnetic (FM) exchange, and has been shown to undergo two magnetic phase transitions, from an incommensurate to commensurate ordered state and then to a fully polarized state, upon the application of $\mu_0H = 0.26$ and 0.53 T in-plane fields, respectively [6]. This suppression of the magnetic order with the application of only a relatively weak field was initially believed to indicate the presence of fairly weak non-Kitaev interactions in the material, relative to similar systems, which led to its identification as a proximate KQSL candidate. However, recent experimental studies point to a non-Kitaev, highly anisotropic and geometrically frustrated ground state, better described by the XXZ-J_1-J_3 model, as opposed to the JKΓ model associated with the KQSL [8]. The frustration in BCAO then arises due not to Kitaev-type
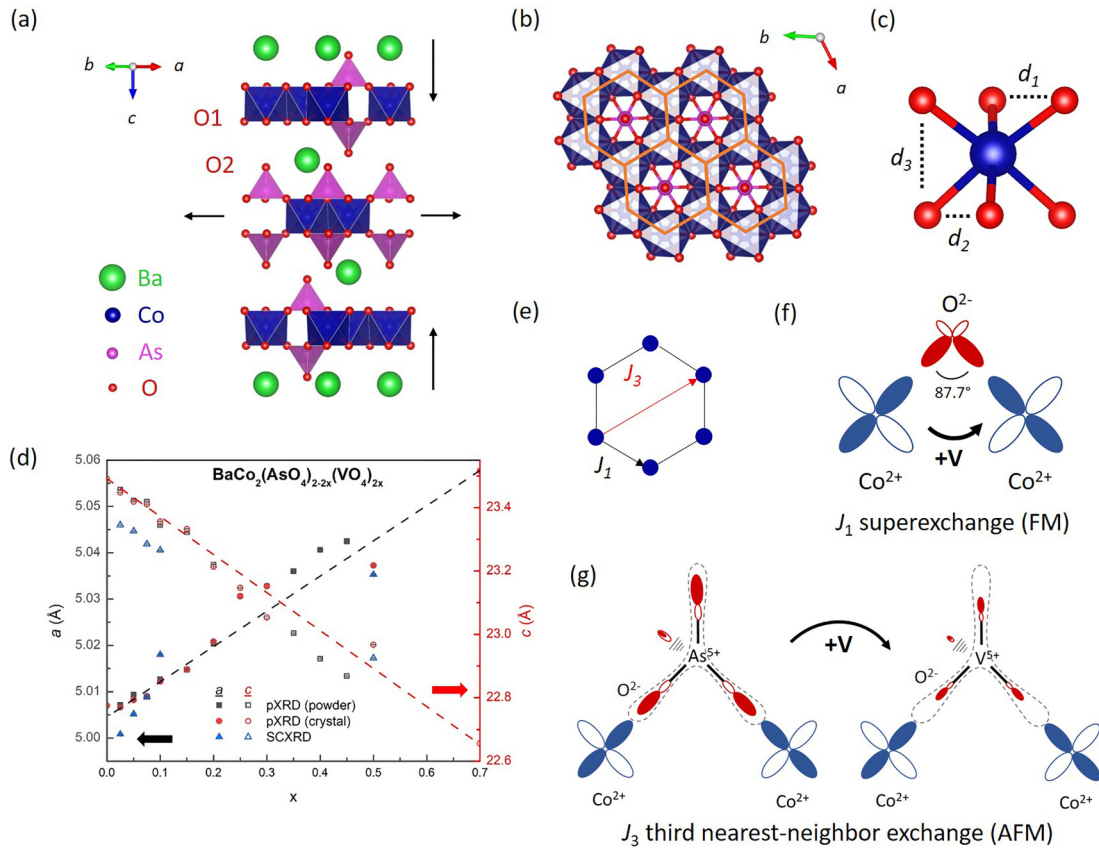
---

*aferren2@jhu.edu
†mcqueen@jhu.edu

FIG. 1. Effects of vanadium substitution on the crystal structure of and exchange pathways in $BaCo_2(AsO_4)_2$. The crystal structure of $BaCo_2(AsO_4)_2$ (BCAO) projected (a) within the ab plane and (b) along the stacking axis. (c) Trigonal distortion of the cobalt octahedra within the honeycomb layer in pure BCAO, defined as $\frac{2d_3}{(d_1+d_2)}$. For an ideal octahedron, this value is equal to 1. (d) Calculated shifts in the a and c lattice parameters as a function of nominal V substitution for As. Lattice parameters for each composition were derived from Rietveld refinement of once- (black) and twice-heated (red) pXRD data, as well as from refinement of twice-heated SCXRD data (blue). General trend lines are shown in black (a) and red (c). The calculated lattice parameter shifts for the nominally $x = 0.50$ sample are lower than would be anticipated from the broader trends observed, indicating that more V was lost in the course of this synthesis. (e) Dominant superexchange J_1 and third nearest-neighbor J_3 exchange pathways within the honeycomb plane described by the XXZ-J_1-J_3 model of geometric frustration. (f) Orbital diagram of the J_1 superexchange pathway. On increasing V substitution, this angle would be expected to increase and the magnitude of J_1 expected to decrease, relative to that of pure BCAO. (g) Orbital diagram of the J_3 third nearest-neighbor exchange pathway. On increasing substitution of the strongly covalently bonded arsenate group with the more ionically bonded vanadate, exchange along this pathway is expected to weaken, reducing J_3.

bond-dependent interactions, but rather due to competition between ferromagnetic superexchange (J_1) and third nearest-neighbor antiferromagnetic (J_3) exchange between Co^{2+} ions in the honeycomb plane [Fig. 1(e)].

While its promise as a quantum spin liquid candidate is ultimately dampened by the fact that it magnetically orders, the closeness of BCAO to the ideal octahedral Co^{2+} geometry was initially believed to indicate that the material itself may be chemically tuned to exhibit more ideal QSL behavior. In order to do so without otherwise disrupting the honeycomb geometry of the cobalt layer, two potential avenues for improvement via chemical substitution exist. The substitution of some small percentage of either the interlayer polyanion group (AsO_4^{3-}) or alkaline earth atom (Ba^{2+}) may alter the local Co^{2+} coordination environment enough to produce more perpendicular Co-O-Co bond angles, and subsequently more perfect octahedral coordination, that would allow for maximal

Kitaev and minimal Heisenberg exchange in the honeycomb plane. In particular, substitution of the interlayer polyanion group is expected to more strongly influence the third neighbor exchange interaction J_3, and thus also the degree of frustration in the XXZ-J_1-J_3 model.

Of the divalent, reliably nonmagnetic ions, partial substitution of the 12-fold coordinate Ba^{2+} would likely only be possible with either Sr^{2+} or Pb^{2+}, both of which would represent a roughly 13% reduction in ionic radius—an increase in size, at least with simpler ions, would not be possible. A pure Pb analogue of BCAO is not known to exist, and the reported $SrCo_2(AsO_4)_2$ phase does not contain Co on a honeycomb lattice [9]. More flexibility exists for partial As substitution, with tetrahedrally coordinated V^{5+}, P^{5+}, Sb^{5+}, and Nb^{5+} all being potentially viable. Of these, only the P-analogue has been previously synthesized, and existing studies thereof have been hindered by the higher stability of two competing poly-

morphs [10]. The maximum amount of substitution without the introduction of major structural deformations would likely occur for V^{5+}, as its tetrahedral metal-oxygen bond lengths are roughly analogous to that of As^{5+}, whereas Nb^{5+} and Sb^{5+} would represent a large increase, and P^{5+} a large decrease, respectively. The fully substituted, tetragonal $BaCo_2(VO_4)_2$ (BCVO) does not contain a honeycomb lattice, but rather one-dimensional chains of Co^{2+} cations which order antiferromagnetically at $T_N = 5.0$ K [11].

Here we report the synthesis and structural and magnetic characterization of a series of V-substituted BCAO compositions $(BaCo_2(AsO_4)_{2-2x}(VO_4)_{2x})$, $0.025 \leqslant x \leqslant 0.70$. At low substitution levels, $0.025 \leqslant x \leqslant 0.09$, long-range incommensurate order in the system is gradually suppressed to $T \approx 3.0$ K, before disappearing down to at least $T = 0.4$ K in the intermediate substitution region. At higher substitution levels, $0.20 \leqslant x \leqslant 0.70$, signs of spin freezing become apparent and the system begins to behave similar to the fully substituted $BaCo_2(VO_4)_2$ phase. The $x = 0.10$ composition appears to represent a critical point between these two regions, displaying signatures of strong spin correlations, minor changes to the cobalt coordination environment, and a suppression of the incommensurate magnetic ground state, likely due to enhanced quantum fluctuations.

II. RESULTS AND DISCUSSION

A. pXRD

Initial attempts at partial arsenic substitution with vanadium in trigonal BCAO [space group $R\bar{3}H$ (148)] resulted in a series of compositions with clear, progressive shifts in both structural and magnetic properties. The powder diffraction patterns measured for each composition, shown in Fig. S1 [12], show shifts to higher 2θ for the majority of $(h0l)$, $(0kl)$, and $(00l)$ reflections, and a slight shift to lower 2θ for the singular $(hk0)$ reflection around $35.8°$. Assuming random incorporation of vanadium into the structure, Rietveld refinement of the experimental pXRD and SCXRD data in the $R\bar{3}H$ space group resulted in similarly good fits for all compositions upon initial and secondary heating (Tables S1–S4 and S5– S10). Several compositions initially possessed a small ($\sim$3–5 wt%) $Ba_3(AsO_4)_2$ impurity phase, which was typically removed via a secondary heating step above the materials' melting point. Reflections corresponding to this impurity phase were also observed to shift with increasing nominal V substitution of the target phase, indicating that partial substitution of arsenic with vanadium occurs for both phases present in the initial product mixture. Up to $x = 0.70$, the roughly 0.02 Å increase in M-O bond lengths for tetrahedrally coordinated vanadium is observed to produce a gradual contraction of the unit cell along the c axis, as well as a gradual expansion of the a axis, by 0.835 and 0.054 Å, respectively [Fig. 1(d)]. Compared to BCAO, these relative shifts $\Delta c/c = -3.6\%$ and $\Delta a/a = 1.1\%$ correspond to a volumetric contraction of $\Delta v/v = -1.4\%$. When substituted for the arsenate groups present in pure BCAO, the longer V-O bond lengths in the BCAO-V compositions produce a compression of the interplanar region along the stacking axis, which in turn increases steric pressure about the honeycomb plane.

Beyond $x = 0.70$, the tetragonal structure of the pure BCVO phase [space group $I4_1/acd$ (142)] begins to appear, with slight shifts in the observed reflections due to partial arsenic substitution for vanadium, and the trigonal BCAO structure gradually disappears. Similar to previous reports of vanadium substitution for phosphorus in $BaCo_2(PO_4)_2$ (BCPO), the effective upper limit of vanadium uptake in the trigonal BCAO phase appears to be around 70% [13].

More subtle structural changes on increasing vanadium substitution can be observed in the refined SCXRD data (Table S11) [12]. Relative to pure BCAO, the average Co-O-Co bridging angle between neighboring Co^{2+} ions widens from $87.66(7)°$ to $88.31(5)°$, an increase of 0.7% [Fig. S2(a)] [12]. The average Co-O-As bridging angles decrease by -0.6% and -0.2%, respectively, up to $x = 0.50$ [Fig. S2(b)] [12]. As the arsenate/vanadate groups in the structure are directly bound to the honeycomb plane and are pushed closer to it as the unit cell contracts along the stacking axis, these minor changes in bond angles also produce small changes to the local Co coordination environment. Taken as two times the distance between oxygen atoms in the two triangular planes comprising the Co octahedra, d_3, divided by the sum of the O-O distance within each triangle, d_1 and d_2, the trigonal distortion observed in pure BCAO is observed to monotonically decrease by 15% from $0 \leqslant x \leqslant 0.10$ and by a total of 33% by $x = 0.50$ [Fig. 1(c)]. However, as pXRD and SCXRD are not local probes, these values represent only the average bond angles and bond lengths found throughout the structure. Laue diffraction patterns of representative BCAO-V single crystals, shown in Fig. S3, were also used to confirm the crystalline quality of each composition and show no signs of twinning or diffuse scattering, up to $x = 0.20$ [12].

As the shifts in both lattice parameters appear to be progressive over the studied composition range and the shift observed along the a axis is small relative to that observed along the c axis, it is likely that vanadium does not substitute for arsenic randomly in the structure, but rather as discrete domains. Attempts to generate accurate unit cells for each composition, particularly at low substitution levels, would thus be dependent on the manner in which these vanadium clusters are distributed throughout the structure. This would also imply a wider distribution of distortions of the cobalt coordination environments, producing a more complex magnetic ground state. Due to the difficulty in making this determination concretely, refinements on both pXRD and SCXRD data presented in this work were performed under the assumption of random substitution.

Regardless of the true vanadium distribution, the progressive trends in the pXRD and SCXRD data and color changes in the grown crystals from pink (pure BCAO) to red ($0 < x \leqslant 0.40$) and gradually to black ($x \geqslant 0.40$), together indicate average changes in the crystal field splitting energy of the octahedrally coordinated Co and potentially also in the trigonal distortion thereof.

B. Raman scattering spectroscopy

Representative Raman scattering spectra collected from BCAO-V single crystals provide additional evidence for the gradual tuning of the Co coordination environment upon
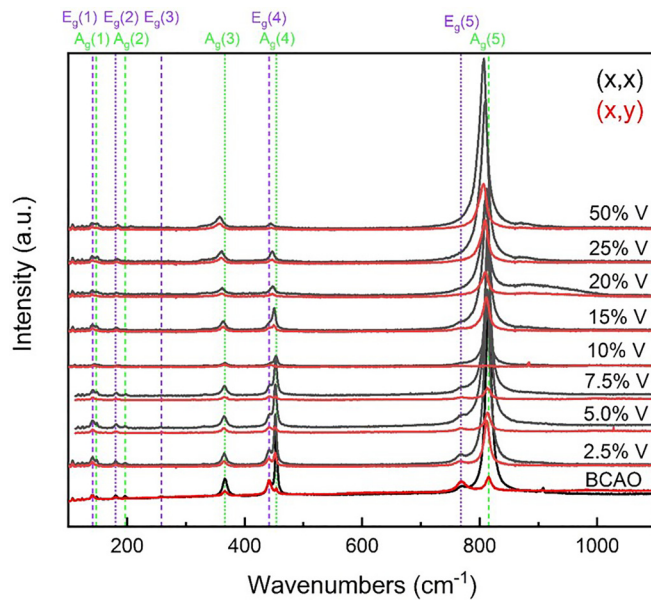
FIG. 2. Nonuniform shifts in vibrational modes on increasing vanadium substitution. Measured Raman scattering spectra of pure and V-substituted BCAO with (x, x–black) and (x, y–red) polarized light. A_g singlet modes are denoted by the green dashed lines, while E_g doublet modes are denoted by the purple dashed lines. A_g singlet modes are largely only active in the (x, x) polarization configuration, while E_g doublet modes appear in both polarization configurations. All sample spectra were calibrated with a silicon standard to ensure a reliable comparison of frequency shifts on increasing vanadium substitution.

substitution of the interlayer polyanion group (Fig. 2). In pure BCAO, the symmetry of the trigonal R$\bar{3}$H structure is well-described by the C_{3i} point group. Of the symmetrically allowed optical modes, 18 are expected to be Raman-active [12 in the (*ab*) plane ($6A_g + 6E_g$)] and 10 of which have been previously observed below 900 cm^{-1} [14]. The polarization dependence of band intensities was used to distinguish between A_g and E_g modes, which were observed to be strongest in the (x, x) and (x, y) configurations, respectively (Fig. S4) [12,14].

Upon partial substitution of As with V, this polarization dependence remains relatively consistent, with singlet A_g modes initially predominating in the parallel polarization (x, x) configuration, doublet E_g modes in the (x, y) configuration, and the overall measured intensity remaining higher for the former. The measured frequency shifts and linewidths for each vibrational mode as a function of substituted vanadium content are shown in Fig. S5 [12]. Up to $x = 0.075$, all E_g and lower-energy A_g modes begin to harden, while the $A_g(5)$ mode begins to soften, all without notable broadening. The higher-energy E_g modes also begin to decrease in intensity.

At $x = 0.10$, the intensity of the measured spectra in both configurations drops considerably, with that of the (x, y) polarization decreasing to less than half of that observed in either the $x = 0.075$ or 0.15 compositions. Interestingly, the intensity of the two highest-frequency $A_g(5)$ and $E_g(5)$ modes decreases by over an order of magnitude relative to the same samples, indicative of more considerable changes to the local

bonding environment in BCAO. While reproducible across several single crystal samples, powder samples of this composition do not possess such a drop in magnitude, as shown in Fig. S6 [12]. This effect likely then arises as a consequence of a distinctive clustering order for the $x = 0.10$ phase that manifests only across larger domains. Beyond $x = 0.10$, most singlet modes begin to soften and the majority of the bands begin to slightly broaden. The higher-energy E_g modes are not observed to shift in frequency, but rather decrease in intensity and are entirely absent by the $x = 0.20$ composition. At and above this level of substitution, the intensity ratio of the remaining A_g and E_g modes is no longer dependent on the experimental configuration and the spectra differ only in magnitude. An additional broad feature also appears at ~875 cm^{-1} at higher substitution levels and is most prominent for the $x = 0.20$ composition. This likely indicates a more heavily disordered bonding environment that introduces greater spin freezing in this region.

Upon chemical substitution, the majority of systems display noticeable broadening of Raman active modes, indicative of random displacement of the substituted atom and subsequently higher disorder throughout the material [15,16]. While slight broadening of several modes is observed upon increasing V substitution of BCAO, the bands remain comparatively sharp, indicating that vanadium does not purely substitute randomly and further supporting that it may do so in a periodic manner.

Although not explicitly assigned in previous reports, the highest frequency of these likely correspond to breathing modes of the two distinct oxygen sites present in the structure [17]. The frequencies at which these modes appear agree well with those previously attributed to honeycomb lattice materials containing edge-sharing Co octahedra [17,18]. As increasing vanadium incorporation is accompanied by a larger contraction of the unit cell along the stacking axis than expansion within the honeycomb plane, the oxygen vibrations occurring between cobalt layers would be expected to be more substantially impacted by greater substitution. The most impacted, highest-energy oxygen modes [$A_g(5)$ and $E_g(5)$] are thus attributed to the apical oxygen of each arsenate/vanadate group not bound within the honeycomb plane, labeled O2 in Fig. 1(a). The lower frequency oxygen modes [$A_g(4)$ and $E_g(4)$], then correspond to the oxygens directly bound to Co atoms, labeled O1 in Fig. 1(a). In the absence of broader structural change, these modes would be less impacted by substitution outside of the honeycomb planes.

The anomalous frequency and linewidth trends observed for vibrational modes in the $x = 0.10$ composition, combined with the sharp decrease in measured intensity, provide evidence for a critical point at which signs of a more symmetric bonding environment emerge, despite the retention of the trigonal R$\bar{3}$H structure suggested by the diffraction data. Whereas the gradual shifts observed in the calculated lattice parameters for each composition provide evidence for the amount of vanadium substituting into the BCAO structure, this critical point illustrates that the way in which that vanadium is incorporated is not consistent throughout the series. This composition clearly delineates the BCAO-V series between regions of order and disorder, driven by increased steric pressure about the honeycomb plane.
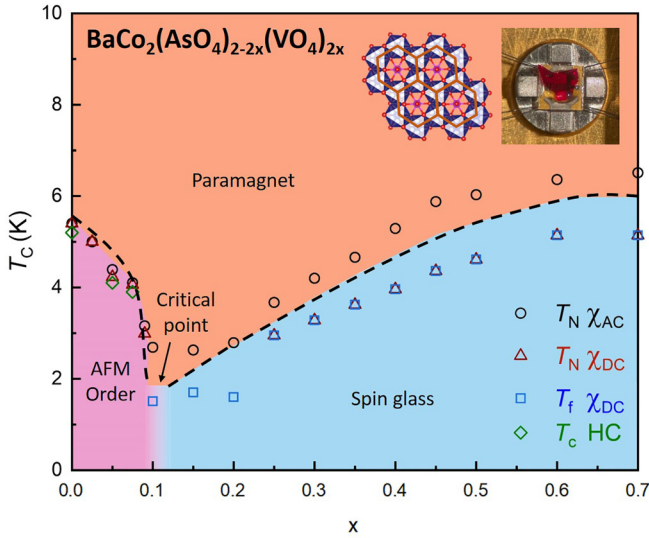
FIG. 3. Magnetic phase diagram of the $BaCo_2(AsO_4)_{2-2x}(VO_4)_{2x}$ ($0 \leqslant x \leqslant 0.70$) series. Derived from AC (T_N–black circles) and DC (T_N–red triangles; T_f–blue squares) magnetic susceptibility, as well as heat capacity (T_C − green diamonds) measurements of representative BCAO-V powder and in-plane ($\mu_0 H \perp c$) single crystal compositions. In the region from $0.025 \leqslant x \leqslant 0.09$, all measurements suggest a gradual suppression of the incommensurate order observed in pure BCAO without the introduction of considerable glassiness. Above $x = 0.20$–0.25, the system begins to behave gradually more like the parent $BaCo_2(VO_4)_2$, displaying an increase in all measured critical temperatures to above that observed in either parent material. In the intermediate range, $0.10 \leqslant x \leqslant 0.20$, the system typically shows no sign of a transition to a long-range incommensurate state in the measured DC susceptibility, while still possessing weaker magnetic transitions in both AC susceptibility and heat capacity measurements. As the system is not known to undergo any structural phase transitions in this temperature regime, this likely indicates a suppression of the incommensurate ordered state and higher degree of magnetic frustration and ground state degeneracy for compositions in this range.

C. Magnetic characterization

Temperature-dependent DC magnetic susceptibility measurements of V-substituted BCAO powder compositions, the ordering transition temperatures of which are shown in red in Fig. 3, suggest a gradual tuning of the magnetic ground state of the system with increasing vanadium content. In pure BCAO, long-range incommensurate antiferromagnetic (AFM) order is suppressed above $T = 5.4$ K. From $0.025 \leqslant x \leqslant 0.09$, the observed transition decreases in temperature to $T \approx 3.0$ K, about half that of the parent material. From $0.10 \leqslant x \leqslant 0.20$, no transition is typically observed, but rather the susceptibility rounds off and stagnates, down to at least $T = 0.4$ K. The relatively broad freezing transition observed for these compositions is suggestive of a large distribution of glass temperatures, distinct from the behavior of a typical spin glass. Above $x = 0.20$, a sharper glassy transition appears and gradually increases in temperature to match the AFM ordering transition observed in the fully substituted end-member BCVO with the dominance of the tetragonal-type phase. The

TABLE I. Fitting parameters obtained from analysis of BCAO-V single crystal magnetization measurements ($\mu_0 H \perp c$) from $T = 150$–300 K.

x	DC T_N (K)	AC T_N (K)	T_f (K)	θ_{CW} (K)	p_{eff} (μ_B)	χ_0	$\chi_\perp/\chi_\parallel$
0	5.40	5.40	–	33.8	5.67	–	62
0.025	5.00	5.00	–	34.9(1)	5.61(1)	−0.002	8
0.05	4.23	4.39	–	37.5(1)	5.70(1)	−0.002	18
0.075	4.06	4.10	–	36.1(2)	5.63(7)	−0.002	34
0.10	–	2.69	1.51	41.8(1)	5.29(1)	0	25
0.15	–	2.63	1.70	39.8(1)	5.31(1)	0	37
0.20	–	2.79	1.60	36.1(1)	5.52(1)	−0.002	40

relative sharpness of this feature in the higher-substituted compositions compared to those in the region of the critical point suggests a smaller distribution of glass temperatures.

To better understand how the magnetic ground state of the system evolves with increasing vanadium content, particularly for the low ($x = 0.025$–0.20) V-substituted samples, temperature-dependent DC magnetic susceptibility measurements were also performed on single crystals of these compositions. With the field applied within the honeycomb plane ($\mu_0 H \perp c$, Fig. S9 [12]), the incommensurate ordering transition declines to $T = 4.06$ K in the $x = 0.075$ sample, slightly higher than that observed in the powder measurements. At and above $x = 0.10$, the susceptibility instead plateaus below $T = 3.0$ K, indicating that the incommensurate ordered state is suppressed in these compositions. Some variability is observed for samples of the $x = 0.10$ composition, with a weak antiferromagnetic transition sometimes appearing between $T = 2.0$–3.0 K before the susceptibility plateaus. As this occurred even for samples from the same batch and other measurement techniques did not show large variability, this can likely be attributed to the proximity of this composition to a critical point. The inherent instability of such a state leaves the magnetic behavior of these samples highly sensitive to a number of synthetic and handling conditions, such as furnace temperature gradient, cooling rate of the melt and sample handling, all of which can produce additional strains and alter magnetic ground state degeneracies. The higher-substituted samples also exhibit a bifurcation between the zero-field-cooled (ZFC) and field-cooled (FC) susceptibility measurements below $T = 2.0$ K, indicating some degree of spin freezing. The ZFC susceptibility for the $x = 0.15$ composition trends negative below T_f, a feature typically attributed to materials containing multiple, highly anisotropic magnetic sublattices [19]. As Co^{2+} is the only magnetic cation present in the BCAO-V system, this composition must possess a higher proportion of discrete cobalt clusters which produce a net negative magnetization at low temperatures.

Curie-Weiss analysis at high temperatures ($T = 150$–300 K) for $\mu_0 H \perp c$ yields a Curie-Weiss temperature $\theta_{CW} \approx 37(1)$ K for all compositions and an effective magnetic moment $p_{eff} \approx 5.5(2)$ μ_B (Table I, Fig. S11), which lies between the effective moments 3.87 μ_B and 6.54 μ_B calculated for the $^4F_{9/2}$ term of the Co^{2+} $3d^7$ ion in the spin only versus the full spin-orbital limits, respectively [12].
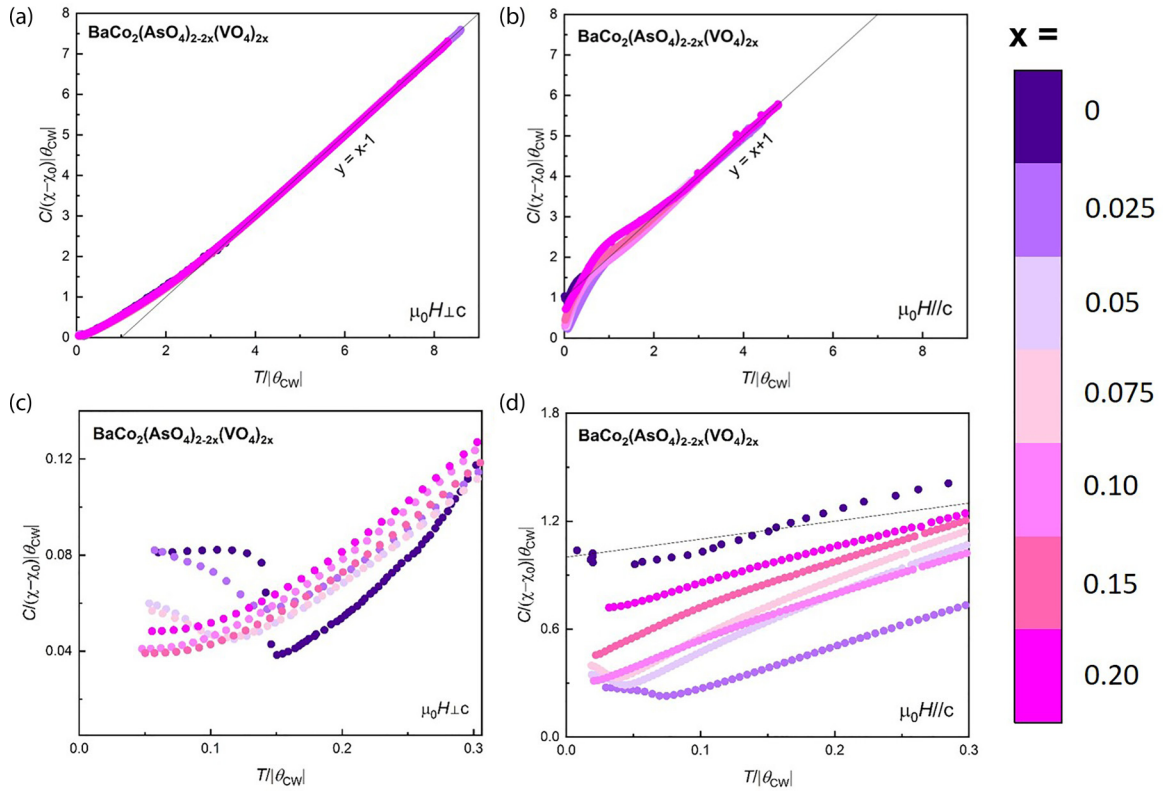
FIG. 4. Evolution of low-temperature deviations from Curie-Weiss behavior on increasing vanadium substitution. Normalized inverse magnetic susceptibility of BCAO-V single crystals, where $C/[(\chi - \chi_0)|\theta|] = T/|\theta| + 1$ for dominant antiferromagnetic (AFM) interactions, and $C/[(\chi - \chi_0)|\theta|] = T/|\theta| - 1$ for dominant ferromagnetic (FM) interactions. Magnetic susceptibility data presented in previous works was extracted and scaled to fit the expected Curie-Weiss behavior at higher T for unsubstituted $BaCo_2(AsO_4)_2$ [6]. When the field is applied (a) within the honeycomb plane ($\mu_0 H \perp c$), FM deviations from ideal behavior dominate in the (c) low-T regime. When the field is applied (b) along the stacking axis ($\mu_0 H \parallel c$), all compositions exhibit AFM deviations from ideal behavior just above their respective T_N, below which FM deviations are observed, which are attributed to the in-plane coupling between neighboring Co^{2+} ions. With increasing V substitution, these (d) low-temperature FM deviations also decrease in magnitude. In both orientations, increasing V substitution is observed to result in a full suppression of the AFM ordering transition by the $x = 0.10$ composition.

Although our low-substitution structural data would suggest a less distorted coordination environment and increase in orbital symmetry on increasing substitution, the Curie-Weiss temperature remains relative stable and positive, and the effective magnetic moment p_{eff} remains close to that of the parent BCAO. Yet for the $x = 0.10$ and 0.15 samples, θ_{CW} is $\approx 20\%$ larger and the effective moment is smaller. This suggests the preservation of dominant FM coupling between adjacent Co^{2+} ions and differs from the expected reduction in quenching of the orbital moment in a more uniform octahedral coordination, possibly due to local clustering of the substituted vanadate groups in the structure. While in cobaltates a non-negligible van Vleck contribution to the magnetic susceptibility is typically observed and would be expected to vary with the degree of the trigonal distortion of the Co octahedra, this should appear as a relatively small, consistent contribution to the effective magnetic moment, given the small change in the trigonal distortion [20]. Although the substitution of the apical polyanion groups would not be expected to greatly impact the in-plane magnetic exchange pathways, these results, as well as the observed structural changes, indicate modification of both the FM J_1

and the AFM J_3 exchange interactions and the degree of distortion of the cobalt octahedra.

When the field is instead applied along the stacking axis ($\mu_0 H \parallel c$), more substantial changes are observed in the measured DC magnetic susceptibility and calculated Curie-Weiss parameters (Fig. S10 [12]). As in the in-plane measurements, increasing vanadium substitution results in a suppression of the incommensurate ordering transition to $T = 4.06$ K by $x = 0.075$, beyond which the susceptibility plateaus below $T = 3.0$ K. Curie-Weiss analysis of the high-temperature susceptibility results in negative θ_{CW} of variable magnitude, as well as reduced effective magnetic moments, relative to pure BCAO (Table S13 and Fig. S11 [12]). All derived θ_{CW} for compositions in this range are smaller than that of the parent phase. The θ_{CW} for both the $x = 0.025$ and 0.20 crystals, $T = -67.8$ and -62.8 K respectively represent local minima in the series. Changes in superexchange pathways as well as in the spin-orbital crystal field levels could both be important factors. With increasing substitution, the effective moment p_{eff} is more variable, however generally trends downward. This may arise due to the variable number of distinct cobalt coordination environments created as progressively more vanadium

is incorporated into the structure. A wider distribution of coordination environments would possess more variability in the average degree of orbital quenching amongst Co^{2+} ions in each honeycomb layer and potentially a lower net effective moment as a result.

A clearer comparison between the observed trends in relative magnetic interaction strength for spin components within and perpendicular to the honeycomb plane can be drawn from the Curie-Weiss-normalized temperature-dependent magnetic susceptibility of each composition, where $C/[(\chi - \chi_0)|\theta|] = T/|\theta| + 1$ for dominant AFM interactions, and $C/[(\chi - \chi_0)|\theta|] = T/|\theta| - 1$ for dominant FM interactions (Fig. 4). For all compositions, spin components parallel to c exhibit AFM deviations from Curie-Weiss behavior above the respective T_N, below which FM deviations are observed. These low-temperature deviations are attributed to the development of net AFM planar spin correlations, and decrease in magnitude with increasing vanadium substitution. When the field is applied within the honeycomb plane ($\mu_0 H \perp c$), FM deviations from Curie-Weiss behavior dominate for temperatures above $T \approx 150$ K. Below this temperature, AFM correlations become more prevalent. The full suppression of the incommensurate AFM ordering transition for the $x = 0.10$ composition is apparent in the absence of a thermal anomaly in both $\chi_{\|c}$ and $\chi_{\perp c}$.

A convenient measure of the magnetic anisotropy and its dependence on substitution and temperature lies in the susceptibility ratio, $\chi_{\perp} c/\chi_{\|} c$, which varies as a function of V-substitution (Fig. S11(c) [12]). At $T = 2.0$ K in pure BCAO, $\chi_{\perp} c/\chi_{\|} c \approx 62$, a value which drops considerably to 8 by $x = 0.025$, before slowly increasing as a function of further substitution. At $x = 0.10$, there is an additional slight decrease in the observed anisotropy. The trends in the magnetization measured along each of the principal axes are however not directly correlated. The magnetization gradually decreases when measured along the stacking axis with increasing V content, while in-plane measurements are relatively consistent, with two sharper declines at $x = 0.025$ and 0.10. As no substitution occurs within the honeycomb lattice, but rather adjacent to it, little variation would be expected in the strength of the J_1 superexchange interactions between neighboring cobalt atoms in the ab plane, though its spin-space anisotropy could change. With substitution of a minimal amount of vanadium into the structure and the corresponding contraction of the unit cell along the c axis, Co^{2+} ions within the honeycomb layer are pushed closer to perfect octahedral coordination. Further incorporation into the parent structure progressively tunes the competing J_1/J_3 exchange interactions, with the $x = 0.10$ composition representing a critical point at which the incommensurate state is suppressed without the introduction of considerable, random glassiness to the system.

One feature commonly observed among magnetic cobaltates is the presence of metamagnetic transitions in field-dependent magnetization measurements, which are associated with the strong anisotropy of the Co^{2+} Kramers doublet ground state [21–23]. In pure BCAO, this manifests as a pair of low-field metamagnetic phase transitions ($\mu_0 H_{c1} = 0.26$ T and $\mu_0 H_{c2} = 0.53$ T) which together produce the dumbbell-shaped hysteresis observed at $T = 1.8$ K [6]. Field-dependent magnetization measurements performed on representative
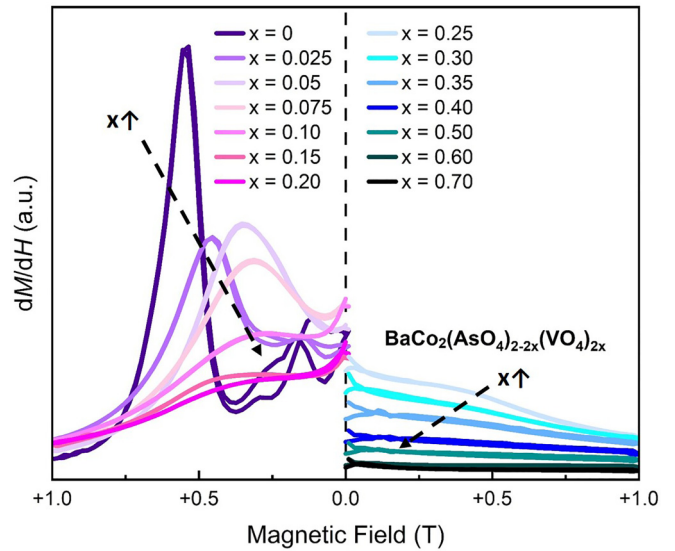

FIG. 5. Evolution of metamagnetism across the BCAO-V powder series. Derivative of field-dependent magnetization with respect to field of representative $x = 0$–0.70 BCAO-V powder samples at $T = 2.0$ K. For each composition, only one magnetization cycle is shown, however the behavior is consistent whether the samples are positively or negatively magnetized to ± 1 T. With increasing V content, both the magnitude and field at which the cobalt metamagnetic transitions occur are observed to decrease, as shown by the black trend lines. No coercivity is observed from $x = 0.025$–0.20. $x \geqslant 0.25$ shown separately for clarity.

BCAO-V powder compositions, shown in Fig. 5 as the derivative of magnetization with respect to the applied field strength, display a clear reduction in both the magnitude and applied field strength at which the Co^{2+} metamagnetic transitions appear. Upon any amount of V substitution, the dumbbell-shaped hysteresis observed in pure BCAO at $T = 2.0$ K is no longer present, with the two metamagnetic transitions gradually merging into one and broadening. At and above $x = 0.25$, minor remanence reemerges and the magnitude of the magnetization drops considerably, relative to pure BCAO. For these glassier compositions, the data likely shows a continuous approach to a fully polarized state, while for $x \leqslant 0.20$, this could be due to the gradual suppression of the metamagnetic transitions to higher fields with substitution. This is indicative of a gradual shift toward more perfect octahedral coordination and an increase in orbital symmetry of the Co^{2+} cations. This would also be consistent with the suppression of the incommensurate ground state observed in pure BCAO. The disorder associated with V substitution may also play a role, as it can impede phase transitions between the long wavelength modulated spin structures associated with the metamagnetic transitions in pure BCAO.

Measurements performed on lower V-content BCAO-V single crystal compositions provide additional insight into the evolution of the observed transitions with increasing substitution. In-plane ($\mu_0 H \perp c$) magnetization measurements (Fig. 6) show no sign of hysteresis in any composition at either $T = 2.0$ or 5.0 K, with all saturating by $\mu_0 H = \pm 1$ T. At $T = 0.4$ K, only a weak remanence is present from $x = 0.10$–0.20, which can likely be attributed to the weak FM coupling
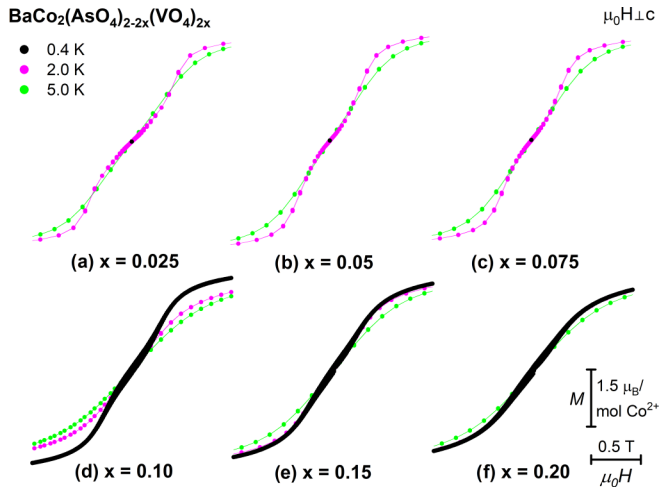
FIG. 6. Suppression of cobalt metamagnetic transitions in BCAO-V single crystals. In-plane, field-dependent magnetization of representative (a) $x = 0.025$, (b) 0.05, (c) 0.075, (d) 0.10, (e) 0.15, and (f) 0.20 BCAO-V single crystals at $T = 0.4$ (black), 2.0 (pink), and 5.0 K (green). Relative to the parent compound, no coercivity is observed for any composition at or above $T = 2$ K, and the cobalt metamagnetic transitions are gradually suppressed. Minor hysteresis is observed for the latter three compositions at $T = 0.4$ K, likely due to the in-plane ferromagnetic exchange between neighboring Co^{2+} ions. All compositions display a saturated magnetic moment by around $\mu_0 H = 1$ T, similar to the parent material.

between neighboring Co^{2+} ions within the honeycomb plane. The two sharp transitions observed in pure BCAO are broadened in all substituted compositions and gradually merge by the $x = 0.10$ sample, leaving only a single smoothed curve. This again indicates some tuning of the average cobalt coordination environment and of the J_1/J_3 ratio upon increasing V content that results in the suppression of the incommensurate ordered state. Out-of-plane ($\mu_0 H \parallel c$) magnetization measurements show only a linear field-dependence and no notable hysteresis at both $T = 2.0$ and 5.0 K, as in the parent material (Fig. S12) [12].

The evolution of the cobalt metamagnetic transitions in V-substituted BCAO is also observed in the in-plane, field-dependent AC magnetic susceptibility data, shown in Fig. S13 [12]. At $x = 0.025$, two transitions are visible at $\mu_0 H = 0.25$ and 0.43 T, with the former being weaker. Upon further substitution, the higher-field transition gradually shifts to meet and merge with that occurring at lower field, in agreement with a gradual suppression of the incommensurate state. The magnitude of the combined transition then continuously decreases with increasing V content. In contrast to the DC magnetization data, the magnitude of the AC susceptibility of several $x = 0.10$ samples also notably decreases, relative to the other compositions, another indication of a more complex interplay between competing exchange interactions at low temperatures.

This discrepancy between the DC and AC response of several compositions is also apparent in temperature-dependent AC magnetic susceptibility measurements of BCAO-V powder samples (Fig. S14) [12]. As in the DC susceptibility, substitution of vanadium for arsenic in BCAO results in a
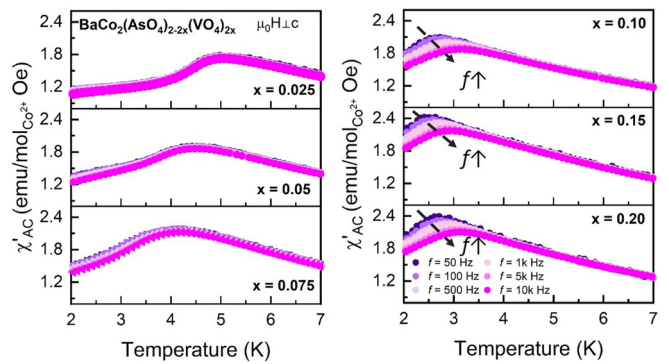

FIG. 7. AC frequency dependence of BCAO-V single crystals on increasing substitution. Real component of the AC magnetic susceptibility of (left–from top to bottom) $x = 0.025$, 0.05, 0.075 and (right–from top to bottom) $x = 0.10$, 0.15, 0.20 BCAO-V single crystal compositions as a function of temperature from $T = 2.0$–7.0 K and with an applied AC field of frequency $f = 50$–10 000 Hz (purple to pink). From $0.025 \leqslant x \leqslant 0.075$, the transition temperature is observed to gradually decrease with increasing x, but is frequency-independent. For these compositions, an increasing frequency dependence is observed only below the transition temperature. Above this level of substitution, an increasing frequency dependence of the transition temperature is observed.

gradual shift in the observed transition temperature, down to $T = 3.6$ K in the $x = 0.075$ composition, albeit with greater broadening. However, from $x = 0.10$–0.20, a narrower transition appears from $T = 2.5$–2.7 K, lower in temperature than other members of the series. Above this level of V substitution, the AC transition begins to weaken, broaden, and shift higher in temperature. When performed on single crystals of the less-substituted compositions, a similar trend appears, with variability again observed in the susceptibility of x = 0.10 samples (Fig. 7). Often samples of this composition possessed sharper transitions, relative to those of the $x = 0.075$ and $x = 0.15$ samples, providing additional evidence for a critical point in this compositional regime.

Notable differences between the magnetic response of a material via AC and DC characterization techniques typically indicate spin glasslike behavior, and subsequently varied spin relaxation rates in a material [24]. In order to better understand the evolution of the magnetic ground state of the BCAO-V system, the temperature dependence of the AC magnetic susceptibility was measured as a function of applied AC frequency for the lower-substituted single crystal compositions (Fig. 7, zoomed view in Fig. S15) [12]. From $x = 0.025$–0.075, there is no frequency dependence to T_N from $f = 50$–10 000 Hz, whereas each of the $x = 0.10$, 0.15, and 0.20 compositions display minimal shifts over the same range. The abrupt shift from the absence to appearance of a frequency-dependent T_N is a common signature of the onset of spin freezing, and when considered with the change observed in the DC susceptibility over the same range further suggests the presence of a critical point between the $x = 0.075$ and 0.15 compositions. Similar to the variability observed in DC susceptibility measurements, samples of the nominal $x = 0.10$ composition display a variable frequency dependence of the AC susceptibility, both within and between batches. The

typical frequency dependence of this composition is similar to that observed in the higher substituted samples, however several crystals closer to the critical point display a reduced dependence. The comparative consistency observed across the other compositions further indicates a proximity to a critical point around $x = 0.10$.

Plotting of this frequency dependence as $1/T$ versus $\ln(\omega)$ yields a linear trend for each of the three higher V-content samples and indicates the presence of some degree of spin freezing (Fig. S16 and Table S14 [12]). While the uncertainty associated with determination of the precise transition temperature produces considerable error in the calculated activation energies and characteristic frequencies for the $x = 0.10, 0.15$, and 0.20 compositions, both trend upward with increasing x. From $x = 0.10$–0.20, linear fitting yields an Arrhenius-type activation energy between $E_a/k_B = 91.8$–107.5 K and a characteristic frequency on the order of $\omega_0 = 10^{16}$–10^{18} Hz, consistent with a cluster glass ground state [25–27]. The magnetic ground state of the BCAO-V system is then likely best understood as a gradual suppression of the incommensurate order down to around $x = 0.10$, followed by the introduction of increased glassiness after its disappearance, as has been commonly reported for phases possessing high degrees of magnetic frustration and substitution-induced disorder [28]. With respect to the interaction strength between magnetic Co^{2+} ions in the BCAO-V structure, the $x = 0.10$ composition then represents a critical point about which strong spin correlations persist down to low temperatures without the transition to the incommensurate state. The bifurcation of FC/ZFC magnetization data for $T \approx 1.48$ K [Fig. S9(d)] indicates some degree of spin freezing at the critical point, as is generally expected in the presence of disorder [12]. In the analogous $BaCo_2(PO_4)_{2-x}(VO_4)_x$ system, similar behavior was attributed to the presence of a spin-liquid-like state stabilized by strong quantum fluctuations [13].

Further evidence for a spin-glass-like ground state in this composition space is observed in the heat capacity of representative BCAO-V polycrystalline samples, shown in Fig. 8. With increasing V content, the transition attributed to the onset of long-range incommensurate order in pure BCAO again substantially broadens and declines in both magnitude and temperature, down to $T \approx 4.0$ K from $x = 0.075$–0.20. In the absence of an applied field, all substituted compositions possess singular broad humps, higher in temperature than the transitions observed in both DC and AC susceptibility. Beyond this level of substitution, the transition shifts higher in temperature, in agreement with that observed in the AC susceptibility measurements and indicative of a smaller distribution of glass temperatures in the system.

Additional hints to the glassy nature of the magnetic ground state in the intermediate substitution regime can be observed in the field-dependent heat capacity of single-crystalline BCAO-V compositions. When the field is applied within the honeycomb plane ($\mu_0H \perp c$), all compositions display a linear trend of further broadening and suppression of the transition to higher temperature, with the application of as small as a $\mu_0H = 0.5$ T field being sufficient to partially suppress the magnetic entropy (Fig. S17) [12]. This provides an additional indication of spin freezing in the magnetic ground state and is consistent with the observed stability
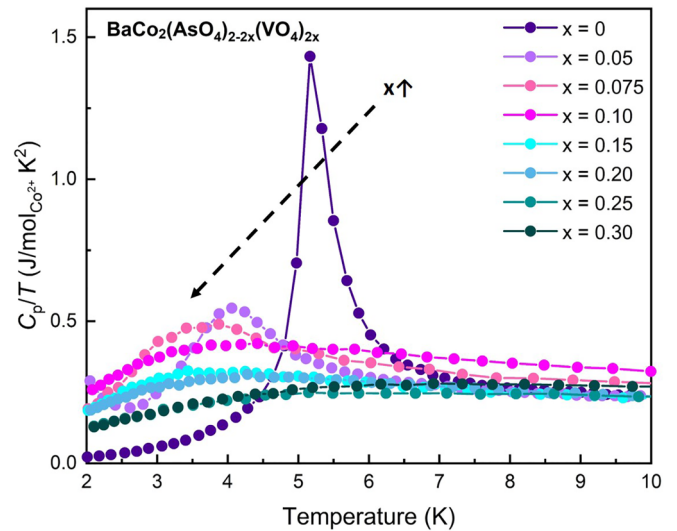

FIG. 8. Suppression of low-temperature heat capacity on increasing vanadium substitution. Representative heat capacity of $x = 0$–0.30 BCAO-V powder samples as a function of temperature from $T = 2.0$–10 K with no applied field. With increasing V content, the magnetic ordering transition declines in both magnitude and temperature down to $x = 0.20$ (as highlighted by the black dashed line). Above this level, the transition begins to shift back to higher temperatures, but remains broad and much weaker than in the parent material.

of the in-plane FM correlations upon V substitution. Conversely, application of the field along the stacking axis yields a more varied response, with progressively larger fields being required for any suppression of the feature to occur (Fig. 9). In the $x = 0.10$ sample, a $\mu_0H = 2.5$ T field is sufficient to
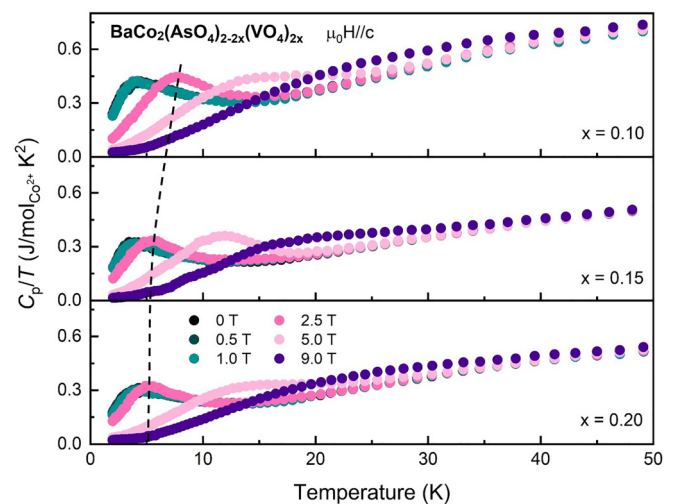

FIG. 9. Increasing barrier to spin reorientation in $BaCo_2(AsO_4)_{2-2x}(VO_4)_{2x}$ ($0.10 \leqslant x \leqslant 0.20$). Representative heat capacity of (from top to bottom) $x = 0.10, 0.15$, and 0.20 BCAO-V single crystals as a function of temperature in a $\mu_0H = 0$–9 T magnetic field applied along the stacking axis. Increasing V content results in a higher barrier to suppression of the magnetic entropy in the system, as indicated by the shifting position of the feature observed for each composition when measured in an applied field of $\mu_0H = 2.5$ T (highlighted by a dashed black line).

suppress the transition by about $\Delta T = 3.9$ K, whereas for the $x = 0.15$ sample, this produces a shift of only $\Delta T = 1.7$ K and for the $x = 0.20$ sample this decreases to $\Delta T = 1.1$ K. However when the applied field is increased to $\mu_0 H = 5.0$ T, the anomaly present for all three compositions is suppressed to a comparable degree. This suggests a finite barrier to spin reorientation which increases from the $x = 0.10$ to the $x = 0.20$ composition, supporting the presence of two distinct ground state phases—the latter behaving as a cluster glass and the former as a more complex intermediate between the regions of order and glassiness bounding the critical point.

Estimates of the magnetic contribution to the measured heat capacity were attempted via subtraction of the nonmagnetic analog of each V-substituted composition. Although $BaMg_2(AsO_4)_2$ and its V-substituted derivatives could be easily synthesized, both direct subtraction and rational scaling of the Mg analogues from the measured heat capacity of the cobalt phases ultimately did not suggest full recovery of the expected magnetic entropy by $T = 50$ K. Subsequent measurement of the Raman scattering spectrum of $BaMg_2(AsO_4)_2$, compared to that of BCAO in Fig. S7, reveals that the substitution of the much smaller Mg atom for Co produces variable, nonuniform shifts in the frequencies of the respective vibrational modes [12]. While the two phases share the same structure, the frequencies of phonon modes in pure and substituted BCAO then differ too considerably for reliable approximation via subtraction of the Mg analogue. However, an estimate of the recovered magnetic entropy for each composition was obtained by scaling of the BMAO-V phase, such that the measured C_p/T converged with that of the Co analogue by $T = 50$ K (Fig. S18) [12]. Integration of this estimated contribution over the same temperature range yields an entropy rise greater than the predicted $\Delta S_{mag} = 1/2 R \ln 2$ for an ideal Kitaev system and less than the $\Delta S_{mag} = R \ln 2$ expected for a typical $S = 1/2$ magnet [29]. Modeling of the evolution of the BCAO phonon spectrum as a function of V substitution will ultimately be necessary to determine the true magnetic entropy rise in this temperature regime.

Reports of other substituted honeycomb phases exhibiting such intermediate spin relaxation rates have typically attributed this behavior to either the presence of stacking faults or magnetic site defects [30]. Due to the higher stability of the high-spin configuration in most Co^{2+} compounds, as well as low likelihood of further oxidation to the Co^{3+} oxidation state upon V substitution, the presence of abundant magnetic site defects is unlikely. In either case, the calculated effective magnetic moment would also be expected to decrease more than is observed. For each composition, the substitution of clusters of arsenic atoms by vanadium would generate distinct stacking sequences within the structure akin to more random stacking faults, leading to more variability in the balance of J_1 superexchange and J_3 third nearest-neighbor interactions within the honeycomb plane. At low substitution levels, this increases the overall degree of geometric spin frustration, while at higher substitution levels this frustration is relieved by typical spin-freezing. Between these two regions, the stacking sequence in the $x = 0.10$ composition produces a near-optimal tuning of the J_1/J_3 exchange interactions, fully suppressing the incommensurate-ordered state before the introduction of more considerable spin freezing.

In solid solutions such as the BCAO-V system, qualitative changes in material properties are typically well described by percolation theory, wherein channels between impurity atoms form above some threshold impurity concentration [31]. These channels produce deviations from the expected trends where impurity atoms enter the structure but largely do not interact with one another. On the two-dimensional honeycomb lattice, this threshold has been reported to be 0.7, which in the BCAO-V series is found to be the upper substitutional limit before transformation to the tetragonal $BaCo_2(VO_4)_2$ structure [32]. However, magnetization and Raman scattering measurements show that the system passes through a critical point around $x = 0.10$, suggesting that standard percolation theory can not be used to effectively describe the evolution of magnetic properties in this system.

Several alternative models of exchange disorder via dilution or magnetic substitution have also been proposed for systems believed to possess dominant Kitaev exchange [33,34]. For the honeycomb iridate family of materials, these models typically agree well with experimental reports, where substitution tunes the magnetic ground state directly from long-range order to that of a typical spin glass. In α-$RuCl_3$, substitution on the ruthenium site initially suppresses the long-range zigzag order before passing through a narrow region of short-range, quasistatic order and finally to the onset of increased spin freezing [35–37]. While substitution in these systems occurs on the magnetic honeycomb lattice, vanadium incorporation into the BCAO structure occurs only on the arsenic site bounding the honeycomb lattice and not for the cobalt within it. As our results are not well-described by any existing model for this type of substitution and direct honeycomb substitution in these related systems has also been claimed to tune the magnitude of off-diagonal exchange, the local minima observed in the $x = 0.10$ composition likely arise from tuning of the J_1/J_3 exchange interactions via exchange disorder.

The impact of increasing disorder on the J_1/J_3 exchange can be understood as both a consequence of the gradual compression of the structure along the stacking axis and a reduction in the covalency of the polyanion orbitals mediating J_3 exchange. In compressing the structure along the c axis, the Co-O-Co superexchange pathway responsible for the dominant FM first neighbor interaction is widened beyond the $87.7°$ observed in pure BCAO [Figs 1(f) and S2(a)]. As predicted by the Goodenough-Kanamori rules, superexchange through an oxygen bridge between half-filled orbitals is expected to be dominant FM when the bridging angle is $90°$ and gradually attain more AFM character as this angle nears $180°$ [38,39]. As more vanadium is substituted into the structure, the average Co-O-Co bond angle widens, reducing the magnitude of the FM J_1 superexchange interaction.

However, the weaker J_3 exchange proceeding through the more complex polyanion group can't be as easily rationalized by these rules [Fig. 1(g)] [8,40]. In pure BCAO, the bounding arsenate group physically bridges third-nearest neighbor Co^{2+} ions via a Co-O-As-O-Co pathway, however due to the large, delocalized orbitals of the arsenic center, bonding in the complex is highly covalent [41]. The polyanion group thus behaves akin to a superatom, with dominant super-exchange-like interactions through the two oxygen atoms linking the cobalt

and arsenic atoms. In BCAO, this interaction is AFM, and the competition between it and the FM J_1 exchange ultimately drives the transition to a long-range incommensurate state at low temperatures. In contrast to the strong covalency of the arsenate group, the smaller vanadate group is bonded more ionically, resulting in reduced orbital overlap and a more complex exchange pathway between third-nearest neighbor Co^{2+} ions [41]. Considering all effects, including the differential d orbital occupation in V^{5+} (d^0) versus As^{5+} (d^{10}), the extent of the vanadate frontier orbital is expected to be much smaller than that of the arsenate, and thus less hopping would occur along this pathway. Increasing the vanadate content of the system would then decrease the magnitude of the AFM J_3 exchange. This is supported by the decrease in the Co-O-As bond angles observed on increasing vanadium substitution [Fig. S2(b)] [12]. While both J_1 and J_3 are expected to decrease with increasing vanadium substitution, the combination of the decrease in Co-O-As bond angle, the more ionic character of the introduced vanadate group, and the subsequently reduced orbital overlap suggests a faster decline in J_3.

When considered in the context of the phase diagram calculated for the honeycomb XXZ-J_1-J_3 model, our results suggest that the ground state of the parent BCAO is not entirely characterized by the double zigzag (dZZ) ordered phase, as has been suggested, but rather on the boundary between it and the zigzag (ZZ) phase [8,40,42]. Taking our results at face value, the incommensurate wave vector observed in pure BCAO likely arises due to the ground state being on the borderline of these regions, and as J_3 is decreased on increasing vanadium substitution, the system is pushed firmly into the dZZ phase stabilized by quantum fluctuations. The expected decrease in J_1 would then represent only small shifts within the same region. This is also consistent with the gradual tuning away of the incommensurate ground state. The evolution of magnetic properties observed across the BCAO-V series must then arise directly from a tuning of the J_1/J_3 exchange, without changing the overall XXZ anisotropy. From our results, we are not able to more specifically place the ground state of the $x = 0.10$ composition on this phase diagram, however given its variable magnetic response, we can infer that it is close to several competing magnetic phases and is likely stabilized by enhanced quantum fluctuations. More extensive inelastic neutron scattering measurements and local structural characterization will ultimately be necessary to determine its true ground state spin configuration, as well as the vanadium clustering that likely gives rise to the critical behavior observed for this composition.

III. CONCLUSIONS

In conclusion, we present the systematic study of the structural and magnetic properties of honeycomb magnet $BaCo_2(AsO_4)_{2-2x}(VO_4)_{2x}$ as it is tuned through a critical

point via partial arsenic substitution with vanadium. At low substitution levels ($0.025 \leqslant x \leqslant 0.09$), magnetic susceptibility measurements show a gradual suppression of long-range incommensurate order in the system, down to $T \approx 3.0$ K. Around $x = 0.10$, the incommensurate order disappears, minor spin freezing is introduced, and both the magnitude of the measured magnetic susceptibility and intensity of the measured Raman bands decrease considerably. Above this level of substitution, greater spin freezing is introduced, long-range order reappears, and the system gradually begins to behave akin to the fully substituted $BaCo_2(VO_4)_2$. With increasing substitution of slightly larger vanadium into the structure, the unit cell shrinks along the c-axis and the relative strengths of J_1 superexchange and J_3 third nearest-neighbor exchange can both be expected to decrease. Around the $x = 0.10$ composition, J_1/J_3 approaches a critical value, producing a local minimum between the regions of long-range, incommensurate order and pure glassiness observed at lower and higher substitution levels, respectively. Likely stabilized by quantum fluctuations, this state represents a compelling example of how magnetically frustrated systems may be chemically tuned to exhibit exotic quantum phenomena and ultimately realize a true quantum spin liquid state.

All data needed to evaluate the conclusions in the paper are present in Ref. [12]. All data underlying this study will be made openly available at the online repository [45].

[1] L. Savary and L. Balents, Disorder-Induced Quantum Spin Liquid in Spin Ice Pyrochlores, Phys. Rev. Lett. **118**, 087203 (2017).

[2] T. Furukawa, K. Miyagawa, T. Itou, M. Ito, H. Taniguchi, M. Saito, S. Iguchi, T. Sasaki and K. Kanoda, Quantum Spin Liquid Emerging from Antiferromagnetic Order by Introducing Disorder, Phys. Rev. Lett. **115**, 077001 (2015).

[3] C. M. Pasco, I. El Baggari, E. Bianco, L. F. Kourkoutis, and T. M. McQueen, Tunable magnetic transition to a singlet ground

state in a 2D van der waals layered trimerized kagomé magnet, ACS Nano **13**, 9457 (2019).

[4] A. Kitaev, Anyons in an exactly solved model and beyond, Ann. Phys. **321**, 2 (2006).

[5] G. Jackeli and G. Khaliullin, Mott Insulators in the Strong Spin-Orbit Coupling Limit: From Heisenberg to a Quantum Compass and Kitaev Models, Phys. Rev. Lett. **102**, 017205 (2009).

[6] R. Zhong, T. Gao, N. P. Ong, and R. J. Cava, Weak-field induced nonmagnetic state in a Co-based honeycomb, Sci. Adv. **6**, eaay6953 (2020).

[7] L.-P. Regnault, C. Boullier, and J. Lorenzo, Polarized-neutron investigation of magnetic ordering and spin dynamics in $BaCo_2(AsO_4)_2$ frustrated honeycomb-lattice magnet, Heliyon **4**, e00507 (2018).

[8] T. Halloran, F. Desrochers, E. Z. Zhang, T. Chen, L. E. Chern, Z. Xu, B. Winn, M. K. Graves-Brook, M. B. Stone, A. I. Kolesnikov, Y. Qiu, R. Zhong, R. J. Cava, Y. B. Kim, and C. Broholm, Geometrical frustration versus Kitaev interactions in $BaCo_2(AsO_4)_2$, Proc. Natl. Acad. Sci. USA **120**, e2215509119 (2023).

[9] D. Osterloh and H. Müller-Buschbaum, Zur kenntnis von $SrCo_2V_2O_8$ und $SrCo_2(AsO_4)_2$/on $SrCo_2V_2O_8$ and $SrCo_2(AsO_4)_2$, Z. Naturforsch. B **49**, 923 (1994).

[10] R. David, H. Kabbour, A. Pautrat, and O. Mentre, Puzzling polymorphism of layered $Ba(CoPO_4)_2$, Inorg. Chem. **52**, 8732 (2013).

[11] Z. He, D. Fu, T. Kyômen, T. Taniyama, and M. Isoh, Crystal growth and magnetic properties of $BaCo_2V_2O_8$, Chem. Mater. **17**, 2924 (2005).

[12] See Supplemental Material at http://link.aps.org/supplemental/10.1103/PhysRevB.108.064433 for experimental materials and methods, compositional analysis, and additional structural, magnetic, and thermal characterization data, which includes Refs. [43,44].

[13] R. Zhong, M. Chung, T. Kong, L. T. Nguyen, S. Lei, and R. J. Cava, Field-induced spin-liquid-like state in a magnetic honeycomb lattice, Phys. Rev. B **98**, 220407(R) (2018).

[14] X. Zhang, Y. Xu, T. Halloran, R. Zhong, C. Broholm, R. J. Cava, N. Drichko, and N. P. Armitage, A magnetic continuum in the cobalt-based honeycomb magnet $BaCo_2(AsO_4)_2$, Nat. Mater. **22**, 58 (2023).

[15] L. Zhang, T. Fujita, F. Chen, D. L. Chen, S. Maekawa, and M. W. Chen, Doping and temperature dependence of raman scattering from $NdFeAsO_{1-x}F_x$ (x = 0–0.2) superconductor, Phys. Rev. B **79**, 052507 (2009).

[16] J. P. Peña, P. Bouvier and O. Isnard, Structural properties and Raman spectra of columbite-type $NiNb_{2-x}V_xO_6$ synthesized under high pressure, J. Solid State Chem. **291**, 121607 (2020).

[17] S. Gohil, K. K. Iyer, P. Aswathi, S. Ghosh, and E. Sampathkumaran, Raman study of $Ca_3Co_2O_6$ single crystals, J. Appl. Phys. **108**, 103517 (2010).

[18] E. Husson, Y. Repelin, N. Q. Dao, and H. Brusset, Normal coordinate analysis of the MNb_2O_6 series of columbite structure (M = Mg, Ca, Mn, Fe, Co, Ni, Cu, Zn, Cd), J. Chem. Phys. **67**, 1157 (1977).

[19] A. Kumar and S. Yusuf, The phenomenon of negative magnetization and its implications, Phys. Rep. **556**, 1 (2015).

[20] H. Liu, J. Chaloupka, and G. Khaliullin, Kitaev Spin Liquid in 3d Transition Metal Compounds, Phys. Rev. Lett. **125**, 047201 (2020).

[21] J. Boonmak, M. Nakano, N. Chaichit, C. Pakawatchai, and S. Youngme, Spin canting and metamagnetism in 2D and 3D cobalt (II) coordination networks with alternating double end-on and double end-to-end azido bridges, Inorg. Chem. **50**, 7324 (2011).

[22] B. Leclercq, H. Kabbour, F. Damay, C. V. Colin, A. Pautrat, A. M. Arevalo-Lopez, and O. Mentré, Metamagnetic transitions versus magnetocrystalline anisotropy in two cobalt arsenates with 1D Co^{2+} chains, Inorg. Chem. **58**, 12609 (2019).

[23] M. Shizuya, M. Isobe, and E. Takayama-Muromachi, Magnetic and electronic properties of misfit-layered cobalt oxide $(Ca_{1-\delta}OH)_xCoO_2$, J. Appl. Phys. **102**, 023704 (2007).

[24] J. Snyder, J. Slusky, R. Cava, and P. Schiffer, How 'spin ice' freezes, Nature (London) **413**, 48 (2001).

[25] K. Binder and A. P. Young, Spin glasses: Experimental facts, theoretical concepts, and open questions, Rev. Mod. Phys. **58**, 801 (1986).

[26] A. Kumar, B. Schwarz, H. Ehrenberg, and R. Dhaka, Evidence of discrete energy states and cluster-glass behavior in $Sr_{2-x}La_xCoNbO_6$, Phys. Rev. B **102**, 184414 (2020).

[27] S. Pakhira, N. Sangeetha, V. Smetana, A.-V. Mudring, and D. C. Johnston, Ferromagnetic cluster-glass phase in $Ca(Co_{1-x}Ir_x)_{2-y}As_2$ crystals, Phys. Rev. B **102**, 024410 (2020).

[28] K. Kovnir, V. O. Garlea, C. M. Thompson, H. D. Zhou, W. M. Reiff, A. Ozarowski, and M. Shatruk, Spin-glass behavior in $LaFe_xCo_{2-x}P_2$ solid solutions: Interplay between magnetic properties and crystal and electronic structures, Inorg. Chem. **50**, 10274 (2011).

[29] S.-H. Do, S.-Y. Park, J. Yoshitake, J. Nasu, Y. Motome, Y. S. Kwon, D. T. Adroja, D. J. Voneshen, K. Kim, T.-H. Jang, J.-H. Park, K.-Y. Choi, and S. Ji, Majorana fermions in the Kitaev quantum spin system α-$RuCl_3$, Nat. Phys. **13**, 1079 (2017).

[30] D. C. Wallace, C. M. Brown, and T. M. McQueen, Evolution of magnetism in the $Na_{3-\delta}(Na_{1-x}Mg_x)Ir_2O_6$ series of honeycomb iridates, J. Solid State Chem. **224**, 28 (2015).

[31] D. Stauffer and A. Aharony, *Introduction to Percolation Theory* (Taylor & Francis, Philadelphia, PA, 1992), pp. 15–56.

[32] H. Scher and R. Zallen, Critical density in percolation processes, J. Chem. Phys. **53**, 3759 (1970).

[33] W. P. Cai, Z. R. Yan, R. M. Liu, M. H. Qin, M. Zeng, X. B. Lu, X. S. Gao, and J.-M. Liu, Magnetic impurity doping induced spin-glass state and short-range zigzag order in the honeycomb iridate Na_2IrO_3, J. Phys.: Condens. Matter **29**, 405806 (2017).

[34] E. C. Andrade and M. Vojta, Magnetism in spin models for depleted honeycomb-lattice iridates: Spin-glass order towards percolation, Phys. Rev. B **90**, 205112 (2014).

[35] P. Lampen-Kelley, A. Banerjee, A. A. Aczel, H. B. Cao, M. B. Stone, C. A. Bridges, J.-Q. Yan, S. E. Nagler, and D. Mandrius, Destabilization of Magnetic Order in a Dilute Kitaev Spin Liquid Candidate, Phys. Rev. Lett. **119**, 237203 (2017).

[36] S.-H. Do, W. J. Lee, S. Lee, Y. S. Choi, K.-J. Lee, D. I. Gorbunov, J. Wosnitza, B. J. Suh, and K.-Y. Choi, Short-range quasistatic order and critical spin correlations in α-$Ru_{1-x}Ir_xCl_3$, Phys. Rev. B **98**, 014407 (2018).

[37] G. Bastien, M. Roslova, M. H. Haghighi, K. Mehlawat, J. Hunger, A. Isaeva, T. Doert, M. Vojta, B. Büchner, and A. U. B. Wolter, Spin-glass state and reversed magnetic anisotropy

induced by Cr doping in the Kitaev magnet α-RuCl$_3$, Phys. Rev. B **99**, 214410 (2019).

[38] J. B. Goodenough, An interpretation of the magnetic properties of the perovskite-type mixed crystals La$_{1-x}$Sr$_x$CoO$_{3-\lambda}$, J. Phys. Chem. Solids **6**, 287 (1958).

[39] J. Kanamori, Superexchange interaction and symmetry properties of electron orbitals, J. Phys. Chem. Solids **10**, 87 (1959).

[40] S. Das, S. Voleti, T. Saha-Dasgupta, and A. Paramekanti, XY magnetism, Kitaev exchange, and long-range frustration in the $J_{\mathrm{eff}} = 1/2$ honeycomb cobaltates, Phys. Rev. B **104**, 134425 (2021).

[41] A. J. Bridgeman and G. Cavigliasso, Density-functional investigation of bonding in tetrahedral MO$_4$ anions, Polyhedron **20**, 2269 (2001).

[42] S. Jiang, S. R. White, and A. L. Chernyshev, Quantum phases in the Honeycomb-lattice J_1–J_3 ferro-antiferromagnetic model, arXiv:2304.06062v2.

[43] K. Momma and F. Izumi, Vesta 3 for three-dimensional visualization of crystal, volumetric and morphology data, J. Appl. Crystallogr. **44**, 1272 (2011).

[44] G. M. Sheldrick, Crystal structure refinement with SHELXL, Acta Crystallogr. C Struct. Chem. **71**, 3 (2015).

[45] https://doi.org/10.34863/n3ds-9s54